

# Structural phase transition and related properties of calcium chalcogenides

P. BHARDWAJ, S. SINGH\*, R. K. SINGH<sup>a</sup>

*High Pressure Research Lab. Department of Physics, Barkatullah University, Bhopal-462026, India.*

<sup>a</sup>*School of Basic Sciences, MATS University, Raipur-492002, India*

The pressure induced phase transition and related properties of calcium chalcogenides (CaX, X=S, Se, Te) have been investigated by using the three body potential (TBP) model, after modifying it including the van der Waals attraction and covalency effects. The modified TBP model has been found to reproduce well the experimentally observed phase transition (B1-B2) pressures and associated volume collapses in these chalcogenides. The present results on phase transitions associated volume collapses, and elastic constants have shown closer resemblance with the results obtained other from more sophisticated theoretical calculations.

(Received April 20, 2010; accepted June 16, 2010)

*Keywords:* Calcium chalcogenides, Volume collapse, Elastic constants, Phase transition.

## 1. Introduction

In recent past, the experimental and theoretical studies of the pressure induced phase transition and associated properties of the materials have attracted the attention of condensed matter physicists. The phase transition occurs from NaCl (B1) to CsCl (B2) structure when the pressure is applied to alkali halides [1-4] and hydrides [5-8] and other materials [9-14]. The high-pressure experiments performed on CaO [9], SrO [10], SrS [11], CaTe and SrTe [12] and Ba chalcogenides [13, 14] show that the heavy alkaline earth chalcogenides (AX) form the second largest group of the partially ionic crystals undergoing B1-B2 transition after alkali halides. The alkaline earth chalcogenides (AX: A=Be, Mg, Ca, Sr, Ba; X= O, S, Se, Te) form a very important closed shell ionic system crystallizing in NaCl-type structure at room temperature conditions except for BeO and MgTe (which crystallize in wurtzite structure) [15] and Beryllium chalcogenides (which crystallize in the zinc-belede structure [16]). The rare earth chalcogenides are technologically important materials having many applications ranging from the catalysis to microelectronics. Also, they have applications in the area of luminescent devices.

Many Physicists have although studied B1-B2 phase transitions in BaX and SrX chalcogenides, but the light and middle AX compounds (A = Ca, Be, Mg) have not been systematically investigated. Among them Ca-chalcogenides seem to be more challenging as they have high cation and anion radius ratio resulting in high phase transition pressures. The high pressure structural studies of these chalcogenites have been performed experimentally using the x-ray diffraction (XRD) technique to reveal the first-order phase transition from the NaCl (B1) to CsCl (B2) phase [17] at pressures 40, 38 and 33 GPa in CaS, CaSe and CaTe, respectively. This XRD technique has

also been used to observe the phase transition ( $P_t$ ) and Pressure-Volume (PV) relationships in CaTe ( $P_t = 35$  GPa) and SrTe ( $P_t = 12$  GPa) [12] which have the smallest cation and anion radius ratio [18] among the AX chalcogenides. The phase transition pressure has also been observed [12-15] to be in between 33-35 GPa in CaTe. The transition pressures of calcium chalcogenides are although higher than SrX, SmX, EuX and BaX, but the volume collapses at the transition pressure in CaSe (8%) and CaTe (4%) are comparatively smaller than those obtained in these compounds. The significantly small volume collapse in CaSe and CaTe has been ascribed to the large disparity in their ionic radii among the heavy alkaline earth chalcogenides and hence the repulsive force between the large ions (anions) resist volume collapse at the phase transition in CaSe and CaTe as remarked by Luo et al [17].

In order to reveal the interesting features exhibited by the high pressure phase transition and Pressure-Volume relations in CaX compounds, several efforts have been devoted using the full potential linearized APW [19], *ab initio* [20], pseudopotential [21, 22] and tight binding [23] theories.

In recent years, extensive investigations have been carried out by Singh and coworkers to describe the high pressure phase transitions and allied behavior of divalent metal oxides [24,25] Calcium [26] and rare-earth compounds [27] using the three body potential (TBP) model. In this TBP model, the three body interactions owe their origin to the quantum mechanical foundation [28,29] and also to the phenomenological approach [30] in terms of the transfer (or exchange) of charge between the overlapping electron shells of the adjacent ions in solids. This TBP approach [30] has been extended to include the Hafemeister-Flygare (HF) type [31] overlap repulsion operative upto the second neighbour ions for describing

the lattice static and mechanical properties of binary ionic solids and alloys [37]. Also, Tosi and coworkers [39] have demonstrated the significance of van der Waals (vdW) attraction due to the dipole-dipole (d-d) and dipole-quadruple (d-q) interactions to describe the cohesion in ionic solids. The vdW interactions are generally ignored in the first principle calculations. Besides, it is noted that Motida [40] has incorporated the effect of covalency to reveal the cohesive and lattice properties of partially ionic crystals. The covalency effect becomes important when compounds are compared under pressure and tend to take more close structure.

Motivated from the above remarks, we thought it pertinent to incorporate the effects of both the vdW attraction [39] and the covalency [40] in the framework of TBP [32, 37] model, probably for the first time, to reveal the high pressure phase transitions and associated properties of partially ionic calcium chalcogenides (CaS, CaSe and CaTe). The consequent formulation of the modified TBP (MTBP) model has been described in section II. The application of this model to predict the phase transition properties of Ca chalcogenides are presented and discussed in the next section.

## 2. Theory and method of computation

### 2.1. MTBP Formalism

The application of pressure is well known to cause an increase in the overlap of the neighboring ions in a crystal and this phenomena, in turn, leads to the transfer (or exchange) of small charge [37] between the overlapping electron shells of the adjacent ions. These transferred (or exchanged) charges interact with all other ions of the

$$U_{B_1}(r) = \frac{-\alpha_m z^2 e^2}{r} - \frac{(12\alpha_m z e^2 f_m(r))}{r} - \left[ \frac{C}{r^6} + \frac{D}{r^8} \right] + 6b\beta_{ij} \exp[(r_i + r_j - r)/\rho] + 6b\beta_{ii} \exp[(2r_i - 1.414r)/\rho] + 6b\beta_{jj} \exp[(2r_j - 1.414r)/\rho] \quad (4)$$

$$U_{B_2}(r') = \frac{-\alpha_m z^2 e^2}{r'} - \frac{(16\alpha_m z e^2 f_m(r'))}{r'} - \left[ \frac{C'}{r'^6} + \frac{D'}{r'^8} \right] + 8b\beta_{ij} \exp[(r_i + r_j - r')/\rho] + 3b\beta_{ii} \exp[(2r_i - 1.154r')/\rho] + 3b\beta_{jj} \exp[(2r_j - 1.154r')/\rho] \quad (5)$$

Here,  $\alpha_m$  ( $\alpha'_m$ ) are the Madelung constants for NaCl (CsCl) structures. C (C') and D (D') are the overall van der Waals (vdW) coefficients [39] corresponding to d-d and d-q interactions for B<sub>1</sub>(B<sub>2</sub>) phases. The values of these coefficients have been evaluated by us using their expressions [27] and following the procedure prescribed by Slater and Kirkwood [41].  $\beta_{ij}$  (j=1,2) ( $=-1+z_i/n_i+z_j/n_j$ ) are the Pauling coefficients [42] with  $z_i(z_j)$  and  $n_i(n_j)$  are the valency and number of the outermost electrons in i(j) (anions) (cations), respectively.  $b$  ( $\rho$ ) are the range (hardness) parameters,  $r$  ( $r'$ ) are the nearest neighbour (nn) separations for NaCl (CsCl) structures.  $r_i$  ( $r_j$ ) are the ionic radii of ions i (j) whose values have been directly taken from ref. [17]. Here,  $f_m(r)$  is the modified form of the three body force parameter ( $f(r)$ ) and includes the effect of

lattice via Coulomb's law and give rise to many body interactions [35-37], whose most significant contribution is the three body interaction (TBI) [37]. A schematic description of this mechanism has been illustrated by Singh [37]. Such an increased TBI effects under compression pose an obvious necessity of their inclusion in the investigation of the high pressure behavior in solids. Also, it is well known that whenever the pressure (or temperature or any other variable) is altered in the crystals, its Gibbs free energy changes smoothly and continuously. The Calcium chalcogenides under pressure have been observed to transform from rocksalt (B<sub>1</sub>) to CsCl (B<sub>2</sub>) phase [12, 17]. The Gibbs free energy to such systems is expressed as

$$G = U + PV - TS \quad (1)$$

with U as the internal (or lattice) energy, which is equivalent to the cohesive energy in equilibrium state. S is the vibrational entropy corresponding to the temperature T, pressure P and volume V of the system. Thus, the Gibbs free energies at T=0 for NaCl (B<sub>1</sub>, real) and CsCl (B<sub>2</sub>, hypothetical) phases can be expressed as [30]

$$G_{B_1}(r) = U_{B_1}(r) + PV_{B_1}(r) \quad (2)$$

$$G_{B_2}(r') = U_{B_2}(r') + PV_{B_2}(r') \quad (3)$$

where  $V_{B_1}$  ( $=2.00r^3$ ) and  $V_{B_2}$  ( $=1.54r'^3$ ) are the unit cell volumes for B<sub>1</sub> and B<sub>2</sub> phases, respectively. The first terms in Eqns. (2) and (3) are the lattice (or cohesive) energies for B<sub>1</sub> and B<sub>2</sub> structures which according to the modified TBP model can be expressed as:

covalency on the lines suggested by Motida [40]. Accordingly, the modified three-body force parameter is given by:

$$f_m(r) = f(r) + f_{cov}(r) \quad (6)$$

with

$$f_{cov}(r) = \frac{4V_{sp}^2 \sigma e^2}{rE_g^3} \quad (7)$$

and

$$\frac{V_{sp}^2}{E_g^2} = \frac{1 - e^*}{12}, E_g = E - I \frac{(2\alpha - 1)e^2}{r} \quad (8)$$

Here,  $V_{sp\sigma}$  is the transfer matrix between the outermost p orbital of anion and the lowest excited state of cation,  $E_g$  is the transfer energy of electron from anion to cation. The static and optical dielectric constants are denoted by  $\epsilon_0$  and  $\epsilon_\infty$ , respectively. The Ziegler effective charge ( $e_s^*$ ) is expressed in terms of the transverse optical ( $\omega_t$ ) phonon frequency at the zone centre, as [40]:

$$(e_s^*)^2 = \frac{9\mu\omega_t^2(\epsilon_0 - \epsilon_\infty)}{4\pi N(\epsilon_\infty + 2)^2} \quad (9)$$

with  $\mu$  as the reduced mass and  $N$  as the Avogadro's number. The value of  $f_{cov}(r)$  has been determined from Eqn. (7) taking the measured values of  $\epsilon_0$ ,  $\epsilon_\infty$ , and  $\omega_t$  directly from ref. [43]. The modified TBI parameter  $f_m(r)$  can be expressed by an exponential analytical function [44]

$$f_m(r) = f_{m0}e^{-r/\rho} \quad (10)$$

dependent on the interionic separation ( $r$ ).  $f_{m0}$  is a redundant parameter.

The space derivatives of  $f_m(r)$  can now be expressed as

$$f_m'(r) = f'(r) + f_{cov}'(r) = -\frac{f_{m0}}{\rho}e^{-r/\rho} \quad (11)$$

The symbols appearing in Eqns. (6-11) have their usual meaning as described by Motida [41].

The lattice energies expressed by Eqns. (4) and (5) consist of the long range Coulomb energy (first term) and the TBI energy modified to include the effect of covalency [41] (second term), the vdW attraction energy is due to d-d and d-q interactions [39] (third and fourth terms) and the overlap repulsive energy is expressed by the HF type [38] repulsion extended upto the second neighbour ions (fifth, sixth and seventh terms). The modified TBP (MTBP) model described by Eqns. (4) and (5) for the NaCl and CsCl phases respectively, contains three model parameters ( $b$ ,  $\rho$ ,  $f_m(r)$ ), namely the range ( $b$ ), hardness ( $\rho$ ) and modified TBI parameter  $f_m(r)$ . Following the procedure prescribed in our earlier papers [25, 45] for choosing an appropriate value of the short-range parameter ( $\rho$ ), we have computed the remaining two parameters ( $b$ ,  $f_m(r)$ ) from the equilibrium condition:

$$(dU/dr)_{r=r_0} = 0 \quad (12)$$

$$\text{and } B = (9kr_0)^{-1} [d^2U/dr^2]_{r=r_0} \quad (13)$$

with  $k$  and  $r_0$  as the crystal constant and equilibrium interionic distance, respectively. The input data ( $r_0$ ,  $B$ ) required for the calculation of these parameters are directly taken from ref. [46]. The values of these model parameters ( $b$ ,  $\rho$ ,  $f_m(r)$ ) have been listed in Table I and used to compute the phase transition pressures and the elastic constants in the following sections.

Table I. Model Parameters of CaS, CaSe and CaTe

Model parameters	CaS	CaSe	CaTe
$b$ ( $10^{-12}$ ergs)	0.321	0.873	0.279
$\rho$ ( $10^{-8}$ )	0.295	0.385	0.389
$f_m(r)$	-0.201	-0.411	-0.602

## 2.2. Phase transition pressures

We have followed the technique of minimization of  $U_{B1}(r)$  and  $U_{B2}(r')$  given by Eqns. (4) and (5) at different pressures ( $P$ ) in order to obtain the interionic separations  $r$  and  $r'$  corresponding to  $B_1$  and  $B_2$  phases associated with minimum energies. We have evaluated the concerned  $G_{B1}(r)$  and  $G_{B2}(r')$  and their differences  $\Delta G (= G_{B1}(r) - G_{B2}(r'))$  at different pressures and plotted them against the pressure ( $P$ ) as shown in Fig.1 for CaS, CaSe and CaTe. The phase transition pressure ( $P_t$ ) is the pressure at which  $\Delta G$  approaches zero. At ambient pressure, these materials crystallize in NaCl ( $B_1$ ) structure and undergo a transition to CsCl ( $B_2$ ) structure upon compression.

We have also computed the relative volume changes  $V(P)/V(0)$  from MTBP model corresponding to the values of  $r$  and  $r'$  at different pressures and plotted them against the pressure in Figs. 2 (a, b, c) for CaS, CaSe and CaTe, respectively. The values of  $P_t$  and  $-\Delta V(P)/V(0)$  along with other results on  $V_t(B_1)/V(0)$  and  $V_0(B_2)/V_0(B_1)$  are depicted in Table II and compared with experimental [12, 17] and theoretical [19-23] results. It is obvious from Table II and Figs. 1 and 2 that our calculated volume collapses,  $-\Delta V(P)/V(0)$ , obtained from MTBP model are 9.8%, 7.2% and 4.3%, which are in closer agreement with their experimental [17] data 10.2%, 7.7% and 4.6%, for CaS, CaSe and CaTe, respectively. The  $-ve$  sign shows the compression in these crystals.

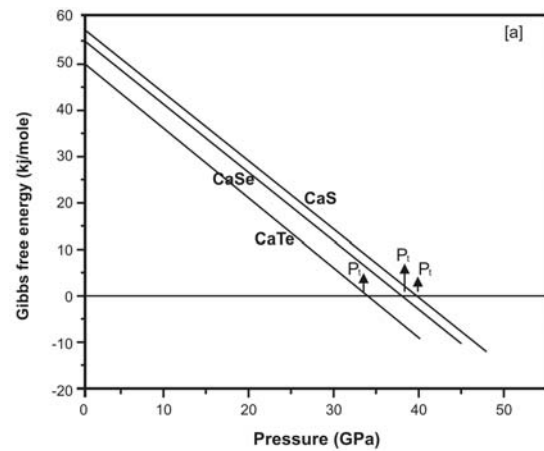


Fig. 1. Variation of  $\Delta G$  (KJ/mol) with pressure ( $P$ ) for CaS, CaSe and CaTe.

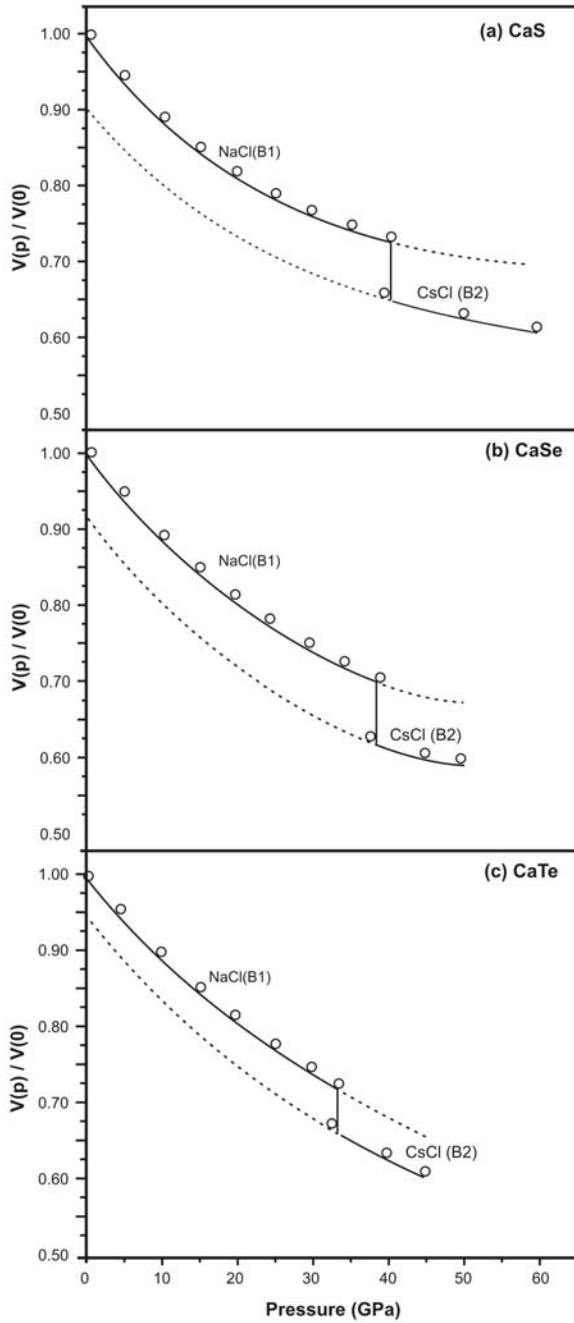


Fig. 2. Variation of volume change  $V(P)/V(0)$  with pressure ( $P$ ) for CaS, CaSe and CaTe.

### 2.3. Second order elastic constants

The expressions for the second order elastic constants (SOECs), derived by following the prescribed procedure [47] and using the lattice energy for B<sub>1</sub> and B<sub>2</sub> structures given by Eqn. (4) and (5), are expressed below for both the NaCl (B<sub>1</sub>) structure as [47]:

$$C_{11} = (e^2 / 4a^4)[-5.112Z(Z + 12f_m(r)) + A_1 + (A_2 + B_2) / 2 + 9.3204zaf'_m(r)] \quad (14)$$

$$C_{12} = (e^2 / 4a^4)[0.226Z(Z + 12f_m(r)) - B_1 + (A_2 - 5B_2) / 4 + 9.3204zaf'_m(r)] \quad (15)$$

$$C_{44} = (e^2 / 4a^4)[2.556Z(Z + 12f_m(r)) - B_1 + (A_2 + 3B_2) / 4] \quad (16)$$

and the CsCl (B<sub>2</sub>) structure as [47]:

$$C_{11} = (e^2 / 4a^4)[-0.7009Z(Z + 16f_m(r)) + \frac{(A_1 + 2B_1)}{6} + \frac{A_2}{2} + 3.1337zaf'_m(r)] \quad (17)$$

$$C_{12} = (e^2 / 4a^4)[-0.6897Z(Z + 12f_m(r)) + \frac{(A_1 - 4B_1)}{6} - \frac{B_2}{2} + 3.1337zaf'_m(r)] \quad (18)$$

$$C_{44} = (e^2 / 4a^4)[-0.3504Z(Z + 12f_m(r)) + \frac{(A_1 + 2B_1)}{6} + \frac{B_2}{2}] \quad (19)$$

Also, the pressure derivatives of these SOECs are expressed for NaCl (B<sub>1</sub>) phase as [47]:

$$\frac{dB}{dp} = -(3\Omega)^{-1} \left[ \begin{array}{l} 13.980Z(Z + 12f_m(r)) + C_1 - 3A_1 + C_2 - 3A_2 \\ -167.7648zaf'_m(r) + 41.9420za^2f''_m(r) \end{array} \right] \quad (20)$$

$$\frac{dS}{dp} = -(2\Omega)^{-1} \left[ \begin{array}{l} 23.682Z(Z + 12f_m(r)) + C_1 + (C_2 + 6A_2 - 6B_2) / 4 \\ -50.0752zaf'_m(r) + 13.9808za^2f''_m(r) \end{array} \right] \quad (21)$$

$$\frac{dC_{44}}{dp} = -(\Omega)^{-1} \left[ \begin{array}{l} -11.389Z(Z + 12f_m(r)) + A_1 - 3B_1 + \frac{C_2 + 2A_2 - 10B_2}{4} \\ + 44.6528Zaf'_m(r) \end{array} \right] \quad (22)$$

with

$$\Omega = -2.330Z(Z + 12f_m(r)) + A_1 + A_2 + 21.9612zaf'_m(r) \quad (23)$$

and for CsCl (B<sub>2</sub>) phase as [47]:

$$\frac{dB}{dp} = -(3\Omega)^{-1} \left[ \begin{array}{l} 2.0350Z(Z + 16f_m(r)) + \frac{C_1 - 3A_1 + C_2 - 3A_2}{2} \\ -56.4032zaf'_m(r) + 24.433za^2f''_m(r) \end{array} \right] \quad (24)$$

$$\frac{dS}{dp} = -(2\Omega)^{-1} \left[ \begin{array}{l} -5.2235Z(Z + 16f_m(r)) + A_1 - B_1 + \frac{C_2}{2} \\ + 47.954zaf'_m(r) \end{array} \right] \quad (25)$$

$$\frac{dC_{44}}{dp} = -(\Omega)^{-1} \left[ \begin{array}{l} -1.2323Z(Z + 16f_m(r)) + \frac{A_1 - 7B_1 + C_1 + 3A_2 - 9B_2}{6} \\ -6.580Zaf'_m(r) + 2.714za^2f''_m(r) \end{array} \right] \quad (26)$$

with

$$\Omega = -0.3392Z(Z + 16f_m(r)) + \frac{A_1 + A_2}{2} + 9.4008zaf'_m(r) \quad (27)$$

where the bulk (B) and shear (S) moduli are expressed as:

$$B = \frac{1}{3}(C_{11} + 2C_{12}) \quad (28)$$

$$S = \frac{1}{2}(C_{11} - C_{12}) \quad (29)$$

The symbols  $A_i$ ,  $B_i$ , and  $C_i$  ( $i = 1, 2$ ) are defined elsewhere [25, 47] and evaluated from the knowledge of the model parameters ( $b$ ,  $\rho$ ) and the vdW coefficients ( $c_{ij}$  and  $d_{ij}$ ) whose values have been estimated by us using their expressions [27, 39] derived from the Slater-Kirkwood variational (SKV) method [41].

### 3. Computed results and discussion

The phase transition pressures illustrated by arrows ( $\downarrow$ ) in Fig. 1 have been listed in Table II and compared with their experimental [12,17] and other theoretical [19,20] results. It is interesting to note from the Table II and Fig. 1 that the phase transition pressures ( $P_t$ ), obtained from the MTBP, are in closer agreement with the experimental data [17] than that reported only for CaTe [12] and they also match almost equally well with other theoretical results [19, 20] obtained from more sophisticated approaches.

Table 2. Phase transition pressure ( $P_t$ ) and Volume collapse ( $-\Delta V(P_t)/V(o)$ ) of CaS, CaSe and CaTe.

Crystal	$P_t$ (GPa)	$(-\Delta V(P_t)/V(o))$ (%)	$V_t(B_1)/V(o)$	$V_o(B_2)/V_o(B_1)$
CaS Present	39.50	9.8	0.722	0.90
	Exp. 40.00 <sup>a</sup>	10.2 <sup>a</sup>	0.73 <sup>a</sup>	0.90 <sup>a</sup>
	Others 37.22 <sup>b</sup> GGA	-	0.72 <sup>b</sup> GGA	-
	35.39 <sup>a</sup> LDA	-	0.71 <sup>b</sup> LDA	-
	45 <sup>c</sup> <i>ab initio</i>	7.7 <sup>c</sup> <i>ab initio</i>	0.71 <sup>c</sup> <i>ab initio</i>	0.904 <sup>c</sup> <i>ab initio</i>
CaSe Present	37.70	7.2	0.695	0.93
	Exp. 38.00 <sup>a</sup>	7.7 <sup>a</sup>	0.70 <sup>a</sup>	0.91 <sup>a</sup>
	Others 34.38 <sup>b</sup> GGA	-	0.74 <sup>b</sup> GGA	-
	40.68 <sup>b</sup> LDA	-	0.68 <sup>b</sup> LDA	-
	45 <sup>c</sup> <i>ab initio</i>	7.1 <sup>c</sup> <i>ab initio</i>	0.69 <sup>c</sup> <i>ab initio</i>	0.911 <sup>c</sup> <i>ab initio</i>
CaTe Present	32.9	4.3	0.723	0.97
	Expt. 33 <sup>a</sup>	4.6 <sup>a</sup>	0.74 <sup>a</sup>	0.95 <sup>a</sup>
	35 <sup>d</sup>	10.8 <sup>d</sup>	0.703 <sup>d</sup>	-
	Others 30.41 <sup>b</sup> GGA	-	0.72 <sup>b</sup> GGA	-
	31.58 <sup>b</sup> LDA	-	0.68 <sup>b</sup> LDA	-
27 <sup>c</sup> <i>ab initio</i>	6.1 <sup>c</sup> <i>ab initio</i>	0.73 <sup>c</sup> <i>ab initio</i>	0.907 <sup>c</sup> <i>ab initio</i>	

a-ref [17], b-ref [19], c-ref [20], d-ref [12]

The compression curves plotted in Fig. 2 (a,b,c) resemble fairly well with the experimental variations [12, 17] depicted by open circles (o) for both the  $B_1$  and  $B_2$  phases for all the Ca chalcogenides. The values of the volume collapses ( $-\Delta V(P)/V(0)$ ) are depicted in Table 2 and Fig. 2 (a,b,c) and compared with the corresponding experimental [12, 17] and other theoretical [19-23] results. It is noted from the Fig. 2 (a,b,c) and Table II that the volume collapses ( $-\Delta V(P_t)/V(0)$ ) at the phase transition pressures obtained from the present (MTBP) model are closer to both the experimental [12,17] and other theoretical [19, 20] results for Ca Chalcogenides. This table also depicts that the values of the relative volume changes  $V_t(B_1)/V(o)$  obtained for  $B_1$  phase from the present model are in agreement with both the experimental results [12, 17] and other theoretical results revealed from GGA [19], LDA [19] and *ab initio* [20] approaches. The values of  $V_o(B_2)/V_o(B_1)$  for  $B_2$  phase revealed from our model are also in good agreement with both the experimental [12] and other theoretical results obtained from *ab initio* calculations [20]. Also, the unusual sequence in phase transition pressure and associated volume collapse in CaTe (see Table 2) revealed from the experimental [12, 17], our and other theoretical [19, 20] results may be linked to the largeness of ionic radii ratio

( $r_A/r_C=2.23$  which is closer to the critical value 2.41) as is pointed out by Luo et al [17].

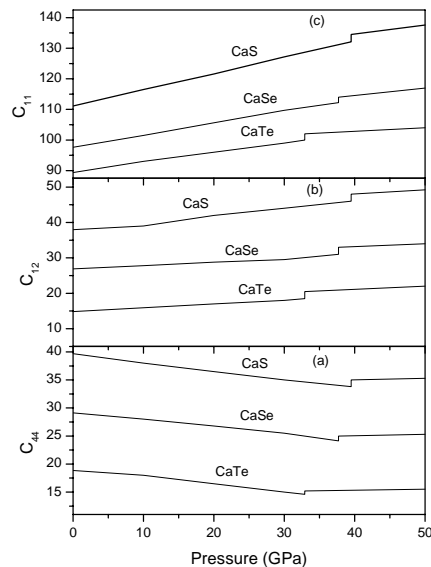


Fig. 3. Variations of elastic constants ( $C_{11}, C_{12}, C_{44}$ ) with pressure ( $P$ ) for CaS, CaSe, and CaTe.

In order to understand the high pressure elastic behavior of Ca Chalcogenides, we have computed the second order elastic constants ( $C_{11}$ ,  $C_{12}$ ,  $C_{44}$ ) for both  $B_1$  and  $B_2$  phases using the Eqns (14-19) and the values of (Ai, Bi, Ci) and depicted their variations with pressure ( $\rho$ ) in Fig. 3 (a,b,c) for both  $B_1$  and  $B_2$  phases. It is noticed from the Fig. 3 (a) that  $C_{44}$  decreases linearly with the increase of pressure and suddenly moves away from zero at the phase transition pressure and again varies linearly for  $B_2$  phase in all Ca chalcogenides. On the contrary,  $C_{11}$  and  $C_{12}$  both increase linearly with the increase of pressure (see Fig. 3 (b,c)) for  $B_1$  phase and steeply rise away from zero at the phase transition pressure and again increase linearly with pressure for  $B_2$  phase. These features are in accordance with the characteristics of the first order phase transitions in these chalcogenides.

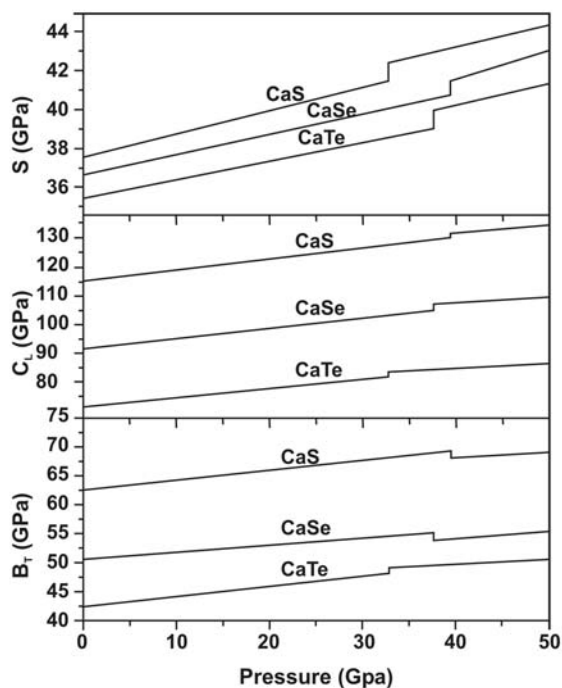


Fig. 4. Variation of Bulk ( $B$ ), Shear ( $S$ ) and elastic stiffness ( $C_L$ ) with pressure ( $P$ ) for CaS, CaSe and CaTe.

In order to judge the validity of these features, we have made further investigations from the variations of the bulk modulus  $B=[(C_{11}+2C_{12})/3]$ , the combination of SOEC elastic stiffness  $C_L=[(C_{11}+C_{12}+2C_{44})/2]$  and the shear moduli  $C_s=[(C_{11}-C_{12})/2]$  and traced them in Fig. 4 (a,b,c). It is found from this figure that their ( $B$ ,  $C_L$ ,  $C_s$ ) values increase linearly with pressure in  $B_1$  phase and suddenly jump to higher values at the phase transition pressure and then increase linearly away from zero in  $B_2$  phase. These characteristics are also in accordance with the first order phase transitions under compression as reported in other chalcogenides [27-31]. The slopes of  $C_s$  increase with pressure in  $B_1$  phase in these chalcogenides and show a

sudden rise in their values at the transition ( $B_1 \rightarrow B_2$ ) pressure and they regain almost similar slope after the transition. Musgrave and Pople [32] have pointed out that if either  $C_{44}$  or  $C_s$  goes to zero with increase of the pressure, then the structure becomes unstable and the crystal is transformed by a spontaneous shear. Thus, it is interesting to note from Fig: 3 that the values of  $C_{44}$  decrease slowly with the increase of pressure in  $B_1$  phase and show discontinuity at the transition to  $B_2$  phase and also their values do not approach zero even beyond the phase transition pressure ( $P_t$ ) which is similar to the trends exhibited by uranium [29, 30] and Mg [31] chalcogenides. This feature of increase in  $C_{44}$  values at the phase transition ( $B_1 \rightarrow B_2$ ) pressure is also exhibited by the results [19] obtained from the first principle (GGA and LDA) calculations performed for Ca chalcogenides and reported in Table 3. This feature revealed by  $C_{44}$  indicates that there occurs the first order phase transition in Ca-chalcogenides. It may, therefore, be concluded that the present model fulfils the shear stability criterion [ ]. The variations of both the bulk modulus ( $B=(C_{11}+2C_{12})/3$ ) and elastic stiffness ( $C_L$ ) with pressure shown in Fig 4 reveals that they increase with pressure upto the phase transition and there is discontinuity at the transition pressure ( $P_t$ ) and they regain the similar slope after the transition to  $B_2$  phase in all these chalcogenides.

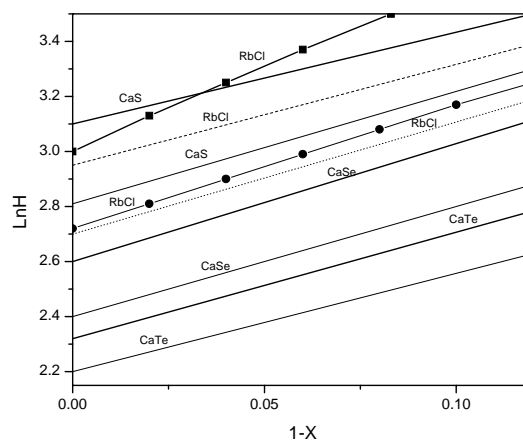


Fig. 5. Equation of states (EOS) for CaS, CaSe and CaTe compared with EOS of RbCl [50, 51]. Thick and thin solid curves represent for  $B_1$  and  $B_2$  phases and line with dash and dot (RbCl) results of Singh et al [51] and Solid Square (line + symbol) and solid circle (line + symbol) (RbCl) represent the results of Recio et al [50] for  $B_1$  and  $B_2$  phases, respectively.

The values of SOECs ( $C_{11}$ ,  $C_{12}$ ,  $C_{44}$ ) and the pressure derivatives of the bulk and shear ( $B$ ,  $C_{44}$ ) moduli have been evaluated using their expressions from Eqns. (14) to (19) and (20) to (26), respectively, for  $B_1$  and  $B_2$  phases. Their values have been listed in Table 3 and compared with their results revealed from GGA and LDA [19] and *ab initio* [20] calculations and the measured data [12, 17]. It is noticed from this table that the results obtained from

MTBP model are generally in closer agreement with the experimental data [12, 17] and are in comparable range with the results obtained from more sophisticated approaches [19-23]. This might be mainly due to the inclusion of the quantum mechanical TBI and covalency effects and the van der Waals attraction in MTBP model.

Although the pressure derivatives,  $S's[=dC_s/dp]_{B1}$  and  $C'_{44}[=dC_{44}/dp]_{B1}$ , could not be compared due to the lack of measured data on them but their values may serve as a guide to the experimental workers in future.

Table 3. Comparison of calculated and experimental values of elastic constants and the pressure derivatives of bulk (B) and shear (S,  $C_{44}$ ) moduli in  $B_1$  and  $B_2$  phases for CaS, CaSe and CaTe.

Compound Phase	Properties	Present work	Expt <sup>a</sup>	GGA <sup>c</sup>	LDA <sup>c</sup>	<i>ab initio</i> <sup>d</sup>	Pseudo potential <sup>e</sup>	Tight binding theory <sup>f</sup>	
CaS	$B_1$	$C_{11}$	111.12	-	108.23	122.87	-	135	202.35
		$C_{12}$	37.98	-	32.01	39.66	-	20	72.42
		$C_{44}$	39.69	-	36.08	41.94	-	38	67.45
		$dB/dP$	4.0	4.2	3.8	4.4	4.1	-	-
		$dS/dP$	6.05						
		$dC_{44}/dP$	-0.511						
	$B_2$	$C_{11}$	117.62		113.60	124.44	-		
		$C_{12}$	39.73		34.20	53.91	-		
		$C_{44}$	42.36		39.01	55.90	-		
		$dB/dP$	3.8		3.5	5.4	4.2		
		$dS/dP$	6.19						
		$dC_{44}/dP$	-0.537						
CaSe	$B_1$	$C_{11}$	97.59	-	95.17	106.76	-	115	155.25
		$C_{12}$	26.88	-	25.56	23.12	-	18	55.75
		$C_{44}$	29.12	-	27.11	29.90	-	31	53.51
		$dB/dP$	3.6	4.2	3.4	4.4	4.1	-	-
		$dS/dP$	5.66						
		$dC_{44}/dP$	-0.451						
	$B_2$	$C_{11}$	100.29		99.78	108.65	-		
		$C_{12}$	28.63		27.22	45.20	-		
		$C_{44}$	34.56		32.46	47.98	-		
		$dB/dP$	4.02		3.8	5.4	4.2		
		$dS/dP$	5.87						
		$dC_{44}/dP$	-0.482						
CaTe	$B_1$	$C_{11}$	89.38	-	89.26	97.42	-		116.96
		$C_{12}$	14.82	-	14.77	17.33	-		45.18
		$C_{44}$	18.86	-	18.52	23.99	-		43.90
		$dB/dP$	3.4	4.3	3.3	4.3	4.2		-
		$dS/dP$	5.12						
		$dC_{44}/dP$	-0.425						
	$B_2$	$C_{11}$	93.86		93.48	111.27	-		
		$C_{12}$	15.12		14.92	17.95	-		
		$C_{44}$	21.02		20.98	26.08	-		
		$dB/dP$	3.9		3.8	4.8	4.2		
		$dS/dP$	5.43						
		$dC_{44}/dP$	-0.502						

a-ref [17], b-ref [12], c-ref [19], d-ref [20], e-ref [21], f-ref [23]

We have further studied the P-V relation using the MTBP model and the Vinet expression [49] for the equation of state:

$$LnH = LnB_0 + (3/2)(B'_0 - 1)(1 - X) \quad (30)$$

with

$$H = PX^2 / 3(1 - X) \quad \text{and} \quad X = V(P)/V(O) \quad (31)$$

The equation of state (EOS) curves representing the  $B_1$  and  $B_2$  phases, computed by us from the Eq. (30), have been depicted in Fig 5 and compared with other theoretical results for Rubidium Chloride (RbCl) reported by both Singh et al [50] and Recio et.al [51]. It is noticed from Fig. 5 that the Vinet type [49] EOS revealed by MTBP model for Ca Chalcogenides are almost similar to those depicted by Singh et.al [50] and Recio et.al. [51] for RbCl.

#### 4. Conclusions

On the basis of an overall discussion, it is found that the modified three body potential (MTBP) model has depicted the structural phase transition ( $B_1 \rightarrow B_2$ ) and related properties of calcium chalcogenides. For the study of the phase transitions in partially covalent chalcogenides, we have incorporated, probably for the first time, the effect of covalency in the TBP model [29-32] along with the van der Waals interactions. We have computed the results on the phase transition pressure, volume collapse, elastic constants, and pressure derivatives of the bulk and shear moduli and found them to reproduce the experimental data [12, 17] and compare well with other more sophisticated theoretical results [19-23] on calcium chalcogenides. After these comparisons, it is found that the pressure of the phase transition and associated volume collapse decreases with increasing order of ionic radii as is demonstrated experimentally by Luo et al [17]. Further, it has been demonstrated that the Vinet type equation of states (EOS) predicted by the MTBP model for these chalcogenides resemble well with EOS of RbCl reported by others [50,51].

Finally, we may conclude that the modified TBP model has evolved more realistic representation of the interaction mechanism to describe the high-pressure phase transition and allied properties of calcium chalcogenides. This might be due to the inclusion of the three body interaction, van der waals attraction and covalency effects in the present model potential. Further improvement is expected with the use of more suitable functional form for modified TBI parameter  $f_m(r)$ . In view of the versatility of the modeling calculations, it may be remarked that the empirical model potentials like MTBP might have their usefulness in describing the structural and physical properties of more complex structures.

#### Acknowledgement

The authors are thankful to the Madhya Pradesh Council of Science and Technology (MPCST), Bhopal for their financial support to this research work. One of us (PB) is thankful to MPCST for the award of the Research Fellowship.

#### References

- [1] W F T Pistorius, Prog. Solid State Chem. **11**, 1 (1976).

- [2] H. H. Demarest, C. R. Cassell Jr., J. C. Jamieson, J. Phys. Chem. Solids **39**, 1211 (1978).
- [3] T. Yagi, T. Suzuki, S. Akimoto J. Phys. Chem. Solids **44**, 135 (1983).
- [4] Sato Y Sorensen J. Geophys. Res. **88**, 3543 (1983).
- [5] S. J. Duclos, Y. K. Vohra, A. L. Ruoff, Phys. Rev. B **36**, 7664 (1987).
- [6] H. D. Hochheimer, K. Stronssner, W. Honle, B. Baranowski, F. Filipek Z. Phys. Chem. **143**, 139 (1985).
- [7] Y. Kondo, K. Asaumi, J. Phys. Soc. Jpn. **57**, 367 (1988).
- [8] Martins J L Phys. Rev. B **41**, 7883 (1990).
- [9] R. Jeanloz, T. Ahrens, H. K. Mao, P. M. Bell Science **206**, 829 (1979).
- [10] Y. Sato, R. Jeanloz J. Geophys. Res. **86**, 11 (1981).
- [11] K. Syassen Phys. Status Solidi (a) **91**, 11 (1985).
- [12] H. G. Zimmer, H. Winze, K. Syassen, Phys. Rev. B **32**, 4066 (1985).
- [13] S. Yamaoka, O. Shimomura, H. Nakazawa, O. Fukunaga Solid State Commun. **33**, 87 (1980).
- [14] T. A. Grzybowski, A. L. Ruoff Phys. Rev Lett. **53**, 489 (1984).
- [15] M. Dadsetani, A. Pourghazi, Phys. Rev. B **73**, 195102 (2006).
- [16] R. Khenata, H. Baltache, M. Rerat, M. Driz., M. Sahnoun, B. Bouhafs, B. Abbar Physica B **371**, 12 (2006).
- [17] H. Luo, R. G. Raymond, G. Greene, K. Ghandehari, Li Ting, A. L. Ruoff Phys. Rev. B **50**, 16232(1994).
- [18] R. D. Shannon, Acta Crystallogr. **32**, 751 (1976).
- [19] Z. Charifi, H. Baaziz, F. El Haj Hassan, N. Bouarissa J. Phys: Condens. Matter **17**, 4083 (2005).
- [20] P. Cortona, P. Masi J Phys.: Condens. Matter **10**, 8947 (1998).
- [21] F. Marinelli, A. Lichanot, Chem. Phys. Lett. **367**, 430 (2003).
- [22] S. Froyen, M. L. Cohen, J. Phys. C **19**, 2623 (1983).
- [23] G. K. Straub, W. A. Harrison Phys. Rev. B **39**, 10325 (1989).
- [24] K. N. Jog, R. K. Singh, S. P. Sanyal Phys. Rev. B **31**, 6047 (1985).
- [25] R. K. Singh, Singh Sadhna Phys. Rev. B **39**, 671; 1989 J. Phys. Soc. Jpn **66**, 1714 (1997).
- [26] Singh Sadhna J. Phys. Soc. Jpn. **71** 2477 (2002).
- [33] Singh Sadhna, R. K. Singh, Gour Atul Central Euro. J. Phys. **5**, 576 (2007).
- [34] Gour Atul, Singh Sadhna, R. K. Singh J. Phys. Chem. Solids **69**, 1669 (2008).
- [35] P. O. Lowding Adv. Phys. **5** 1 1947 Ark. Mat. Astr. Fys. A (Sweden) **35**, 30 (1956).
- [36] S. O. Lundqvist Ark. Fys. (Sweden) **12**, 365 (1957).
- [37] R. K. Singh, Phys. Reports **85**, 259 (1982)
- [38] D. W. Hafemiester, H. F. Flygare J. Chem. Phys. **43**, 795 (1965).
- [39] M. P. Tosi, F. G. Fumi J. Phys. Chem. Solids **23**, 359 (1962); Tosi M P Solid State Physics **16**, 1 (1964).
- [40] K. Motida J. Phys. Soc. Jpn. **55**, 1636 (1986).

- [41] J. C. Slater, K. G. Kirkwood Phys. Rev. **37**, 682 (1931).
- [42] L. Z. Pauling, Kristallogr **67**, 377 (1928).
- [43] F. Kootstra, P. L. de Boeij, J. M. Snijders Phys. Rev. B **62**, 7071 (2000).
- [44] Cochran W CRC Crit. Rev. Solid State Sci. **2**, 1 (1971).
- [45] Singh Sadhna, R. K. Singh, B. P. Singh, S. K. Singhal, R. Chopra Phys. Status Solidi (a) **180**, 459 (2000).
- [46] D. R. Lide (Ed) CRC: 12-21-39, 1995-1996.
- [47] U. C. Sharma and Verma M P Phys. Status Solidi (b) **102**, 487 (1980).
- [48] M. J. P. Musgrave, J. L. Pople, J. Phys. Chem. Solids **23**, 321 (1962).
- [49] P. Vinet, J. Ferrante, J. R. Smith, J. H. Ros, J. Phys. C **19**, L467 (1986).
- [50] J. M. Recio, Martin A Pendas, E. Francisco, M. Florez, L. Victor Phys. Rev. B **48** 5891 (1993).
- [51] Singh Sadhna, R. K. Singh, R. Rai, B. P. Singh J. Phys. Soc. Jpn. **68**, 1269 (1999).

---

\*Corresponding author: drsadhna100@gmail.com